

NH₃-Mediated Reactive Capture and Conversion: Integrating CO₂ Absorption from Flue Gas with CO Production via NH₄HCO₃ Electrolysis

Sujin Kang,[#] Shoutian Sun,[#] Lun An, Jie Zhang, Long Qi, Wenyu Huang, Bin Wang,* Shuang Gu,* and Wenzhen Li*

Cite This: <https://doi.org/10.1021/acscenergylett.5c04265>

Read Online

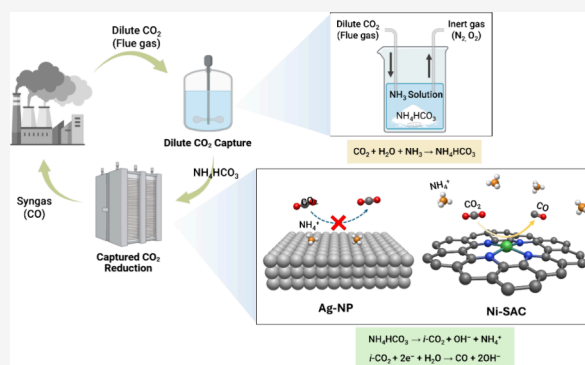
ACCESS |

Metrics & More

Article Recommendations

Supporting Information

ABSTRACT: Efficient carbon capture and utilization require strategies that minimize energy penalties of CO₂ regeneration and compression. Reactive capture and conversion (RCC) address this challenge by integrating capture with direct electrochemical conversion. Here, we show an NH₃-mediated tandem RCC system that couples capture of CO₂ from simulated flue gas (10% v/v CO₂ in N₂) with electroreduction of NH₄HCO₃ to CO over a Ni single-atom catalyst (Ni-SAC). Speciation modeling and capture experiments revealed that a deep CO₂ capture with C/N ratio of 0.65 was achieved using 2.5 M NH₃ from simulated flue gas. Electrolysis of the resulting NH₄HCO₃ on the Ni-SAC delivered an 85% CO Faradaic efficiency at 100 mA/cm² with excellent tolerance to NH₃/NH₄⁺ as confirmed by DFT calculations and ab initio molecular dynamics (AIMD) simulations. Further, the techno-economic analysis established a leveled total cost of CO manufacturing of \$25.43/kmol, gauging the practical viability. Overall, this study holds great potential to decarbonize the chemical manufacturing industry while reducing synthetic production costs.



Efficient carbon capture and utilization (CCU) has been recognized as a key strategy for alleviating global climate change while achieving a carbon-neutral economy.¹ In particular, the reactive capture and conversion (RCC) that integrates CO₂ capture from a dilute gas stream with the subsequent electrochemical conversion into value-added commodity products is among the most attractive CCU approaches, largely because the RCC eliminates the need for CO₂ regeneration and pressurization that is often energy-intensive, process-complicated, and therefore operation-costly.² For example, the CO₂ regeneration and compression steps account for up to 90% of total energy consumption in direct air capture (DAC).^{3,4} Essentially, the capture agent in the tandem RCC system plays a dual role as a process mediator: it first serves as the active medium to absorb dilute CO₂ effectively, after which it turns into a reactant as well as a supporting electrolyte for the succeeding electrochemical conversion. Upon completion of the CCU process, the mediator is regenerated as the capture agent to start the cycle over again.

As a very strong base, aqueous KOH was adopted as the first choice of the RCC mediator for the tandem RCC process, mainly due to the fast reaction with CO₂ from dilute streams forming aqueous KHCO₃ as the intermediate electrolyte (KOH + CO₂ → KHCO₃). With a primary focus on KHCO₃ electrolysis, significant progress has been made in

revamping catalyst designs,^{5–7} optimizing local environments,⁸ and understanding cation effects⁹ for generating value-added products including CO,^{5,7,9–12} formate, and C₂/C₃ chemicals.⁶

Ammonia is a weaker base than KOH, as reflected by the lower pH in their aqueous solutions: 11.6 vs 14 for 1 M NH₃ and 1 M KOH, respectively, under the standard conditions. The reaction heat of CO₂ capture is only 4% weaker (or 2.87 kJ/mol less negative) with NH_{3, aq} than with aqueous KOH: –63.56 kJ/mol of standard reaction enthalpy for NH_{3, aq} + H₂O + CO_{2, gas} = NH₄⁺ + HCO₃[–] vs –66.43 kJ/mol for OH[–] + CO_{2, gas} = HCO₃[–]. Moreover, NH₃ is the second largest commodity chemical with annual production of over 176 million tons,¹³ and green NH₃ can be produced from common agricultural and industrial nitrogen wastes. Therefore, aqueous NH₃ (i.e., NH_{3, aq}, which is distinct from gaseous NH₃, or NH_{3, gas}) was proposed in our recent work as an alternative RCC mediator, and accordingly, aqueous NH₄HCO₃ served as

Received: December 24, 2025

Revised: March 1, 2026

Accepted: March 4, 2026

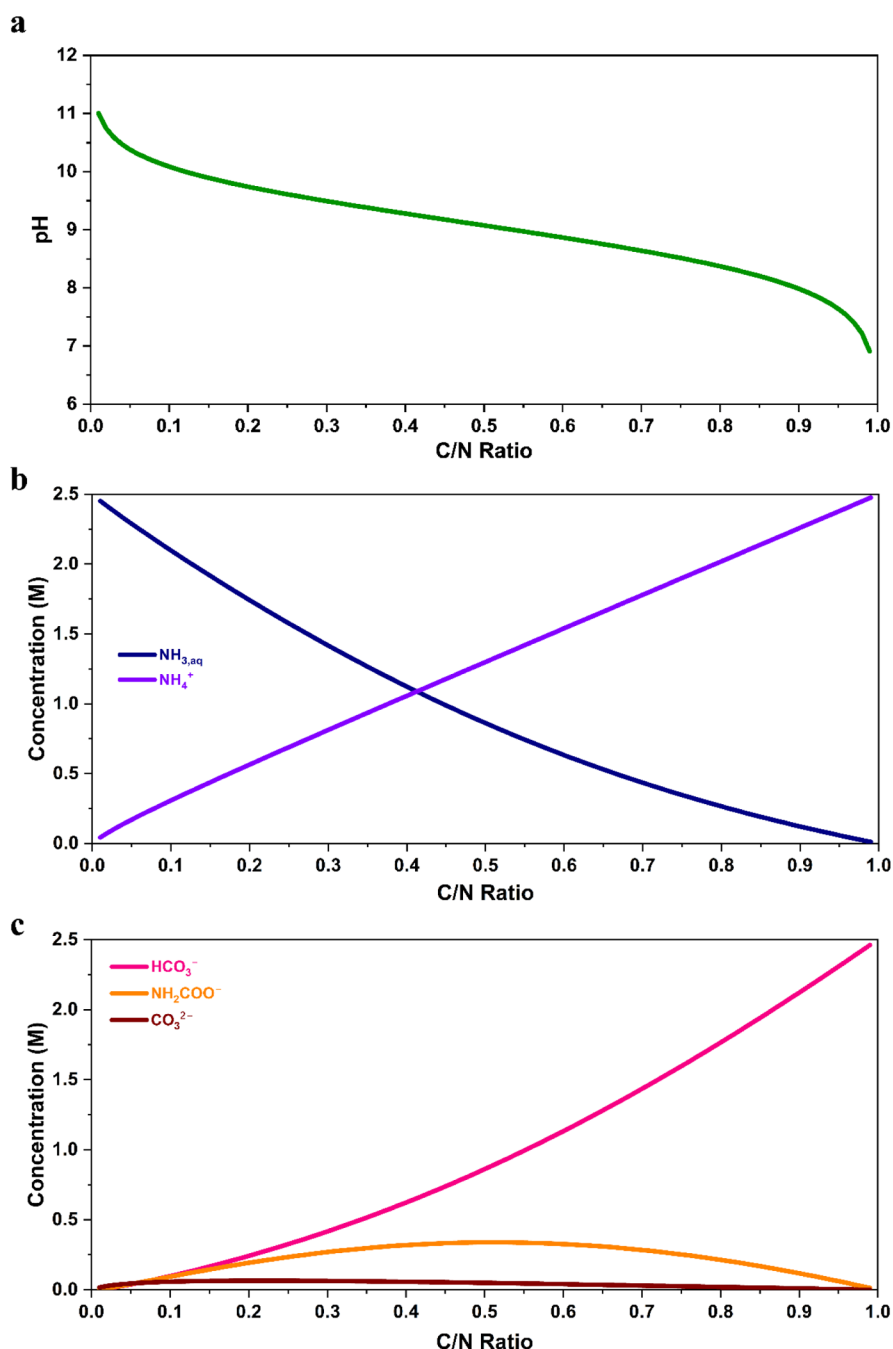


Figure 1. Computed solution pH and concentrations of major ionic species in the H₂O–NH₃–CO₂ system with respect to varying C/N ratio by the numerical method (2.5 M of initial NH₃ solution in water). (a) pH. (b) Concentrations of N-centric species (NH_{3,aq} and NH₄⁺). (c) Concentrations of C-centric species (HCO₃⁻, NH₂COO⁻, and CO₃²⁻).

the intermediate electrolyte that was reduced in electrolysis forming formate (HCOO⁻) as the leading product.^{14,15}

In bipolar membrane (BPM)-based electrolyzers used for tandem RCC, bicarbonate electrolysis proceeds through a mechanism fundamentally distinct from conventional gas- or liquid-fed CO₂ reduction. Protons generated at the BPM via water dissociation create a localized acidic environment at the cathode–membrane interface, where they react with HCO₃⁻ to generate *in situ* CO₂ (i.e., *i*-CO₂) through a local pH swing. The freshly formed CO₂ is then reduced at the cathode catalyst layer supported on a gas diffusion electrode, while OH⁻ ions are produced during CO₂ reduction, regenerating the alkaline capture sorbent. Consequently, the efficiency of bicarbonate

electrolysis is governed by the coupled kinetics of interfacial CO₂ generation and catalytic CO₂ reduction.

Importantly, NH₄HCO₃ was found to substantially promote the CO₂ reduction reaction (CO₂RR) with 23% increased formate-oriented Faradaic efficiency (FE) on a Bi catalyst by releasing tripled *i*-CO₂ at elevated temperatures (such as 40 °C).¹⁴ In addition, the cell voltage was also relieved by 180–240 mV at 100 mA/cm² with NH₄HCO₃ compared with KHCO₃ due to the less negative reversible cathode potential with the lower pH (e.g., 118–177 mV by 2–3 pH units with an OH⁻/e⁻ ratio = 1). For HCO₃⁻-to-CO conversion, the positive shift in reversible potential is even larger: 177–266 mV by 2–3 pH units because of an OH⁻/e⁻ ratio = 1.5.

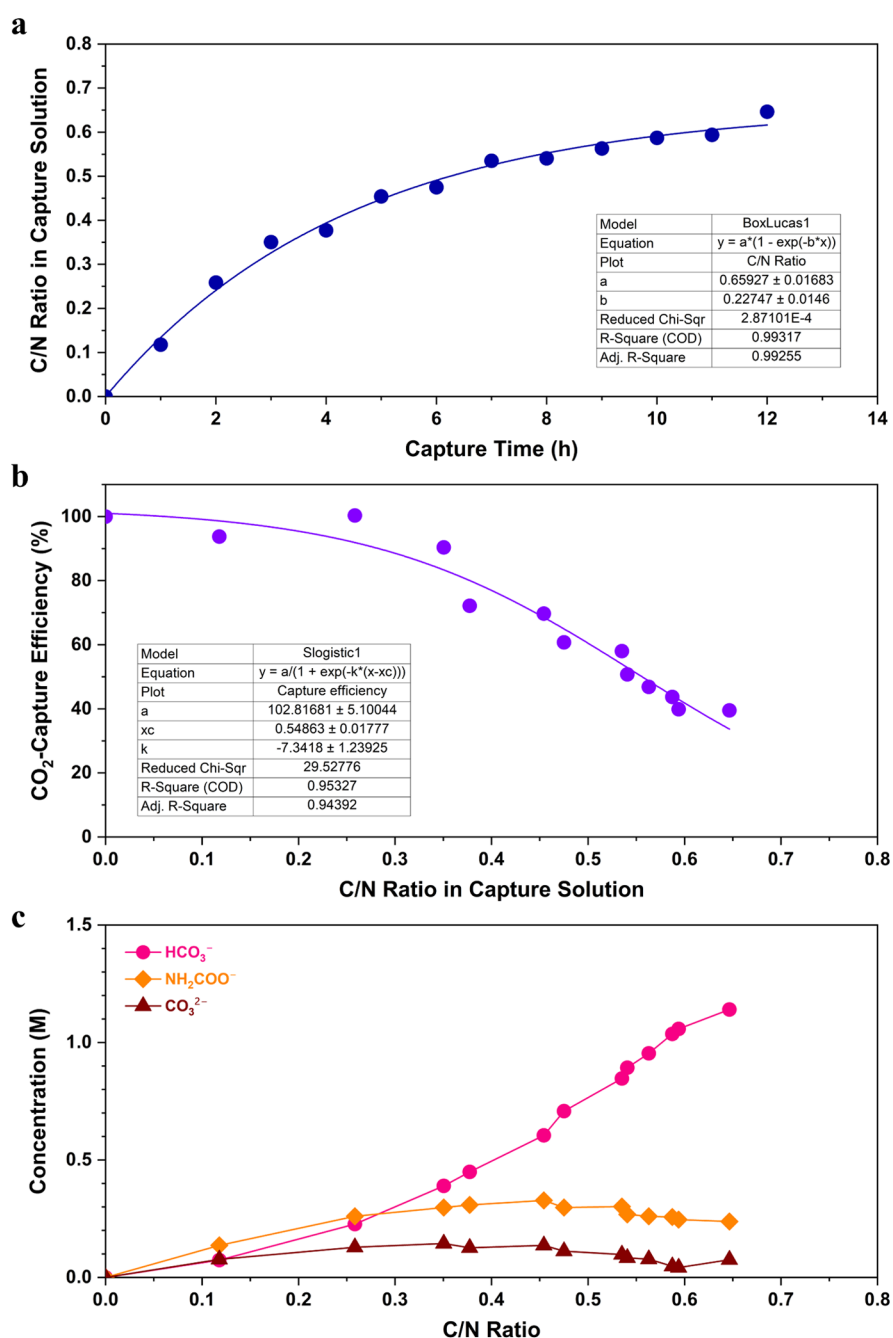


Figure 2. Experimental observation of the CO₂ capture progression in the H₂O–NH₃–CO₂ system (2.5 M initial NH₃ solution in water). (a) C/N ratio observed in the capture solution over the capture time (by ¹³C NMR spectroscopy). (b) CO₂-capture efficiency with respect to the C/N ratio. (c) Detected concentrations of C-centric species (HCO₃⁻, NH₂COO⁻, and CO₃²⁻) as capture products, along with the C/N ratio.

In this work, we present an NH₃-mediated tandem reactive capture and conversion (RCC) process that integrates the capture of CO₂ from simulated flue gas by aqueous NH₃ with selective NH₄HCO₃-to-CO electrolysis on a Ni single-atom catalyst (Ni-SAC). Speciation simulations and ¹³C NMR analyses confirmed the evolution of nitrogen- and carbon-centric species with increasing capture depth, showing good agreement between experiment and theory. While Ag-based catalysts (Ag-NP, OD-Ag) exhibited severe deactivation in NH₄HCO₃ electrolytes—FE_{CO} collapsing from ~27% in KHCO₃ to ≤12%—Ni-SAC maintained excellent tolerance, delivering 85% FE_{CO} in 2.5 M NH₄HCO₃ at 100 mA/cm², surpassing its performance in KHCO₃ (78%) and operating at

80–300 mV lower cell voltages. Mechanistic insights from NH₃-TPD, DFT, and ab initio molecular dynamics (AIMD) revealed that weak NH₄⁺ adsorption and facile desorption on Ni-SAC enable sustained CO₂ reduction in contrast to the NH₄⁺ accumulation on Ag surfaces. Techno-economic analysis further established a leveled CO production cost of \$25.43/kmol, highlighting the practical feasibility of Ni-SAC for scalable ammonia-mediated RCC.

Ammonia has been introduced as a capture agent for CO₂ as early as 1997,¹⁶ given the issues associated with the popular capture agents (e.g., monoethanolamine), including high materials cost and insufficient chemical stability. RCC has emerged as a promising approach to reduce capital expenses,

and the coupling and utilization of dilute CO₂ (such as flue gas) and NH₃ remain largely underexplored. Foremost, it is crucial to understand the complex speciation inside the ternary CO₂–NH₃–H₂O system for guiding the design of the RCC system. In 2006, the speciation in the ternary CO₂–NH₃–H₂O system was quantified by ¹³C NMR spectroscopy with HCO₃[−], NH₂COO[−], and CO₃^{2−} as the three major carbon-centric species from captured CO₂.¹⁷

We first computed the speciation of both nitrogen-centric species (NH_{3, aq} and NH₄⁺) and carbon-centric species (HCO₃[−], NH₂COO[−], and CO₃^{2−}) with respect to the capture depth (C/N ratio) from 0.01 to 0.99 in a typical aqueous ammonia solution (2.5 M) under standard conditions. Specifically, the compositions of ionic species in the aqueous CO₂–NH₃–H₂O ternary system were obtained by numerically solving a group of 7 simultaneous independent equations (encompassing 4 equilibrium equations and 3 conservation equations). Detailed modeling assumptions and computation procedures are shown in the Supporting Information, including standard Gibbs free energies (Table S1), standard equilibrium constants (Table S2), and the numerical solution of ionic concentrations as a function of C/N ratio (Table S3).

The computation results show that the ternary CO₂–NH₃–H₂O system remains almost always alkaline with its pH descending from 11.00 at C/N ratio = 0.01 to 6.91 at C/N ratio = 0.99 (Figure 1a). Specifically, the pH is 9.61 and 9.07 at a C/N ratio = 0.25 and 0.50, respectively. At the same C/N ratio = 0.25, the computed pH (9.61, here) is very close to the reported value (pH = 9.5).¹⁸ As expected, NH_{3, aq} concentration falls while NH₄⁺ concentration rises with an increasing C/N ratio, and they become equal (1.25 M) at the C/N ratio of 0.41 (Figure 1b). When the C/N ratio is between 0.01 and 0.10, all three captured products have comparable concentrations (3.6–98.1 mM, Figure 1c). As the leading captured product, the HCO₃[−] concentration grows monotonously from 3.6 mM at a C/N ratio = 0.01 to 2.46 M at a C/N = 0.99. Interestingly, both NH₂COO[−] and CO₃^{2−} concentrations follow negative parabola-like trends, peaking at 339 mM (at a C/N ratio of 0.51) and at 65.0 mM (at a C/N ratio of 0.22), respectively.

Most previous studies for the flue gas application with NH₃ as a coreactant have been limited to theoretical modeling and process designs; few experimental investigations have been reported.¹⁹ Here, we investigated the capture of CO₂ from a simulated flue gas (10% v/v of CO₂ in N₂) by 200 mL of a 2.5 M NH₃ solution as shown in Figure S1. Production identification was conducted by ¹³C NMR spectroscopy for all carbon-centric species (Figure S2).

The capture depth of C/N ratio = 0.64 was obtained after 12 h of absorption by bubbling at a flow rate of 250 sccm through a simple glass dispenser (25–50 μm in pore size) (Figure 2a). As a measure of CO₂ utilization, the CO₂-capture efficiency was quantified by dividing the total amount of captured carbon in the capture solution by the total amount of supplied carbon element in the gas feed. Nearly complete CO₂ utilization was observed for low C/N ratios (≤0.25), but the utilization dropped quickly when increasing C/N ratio: the CO₂-capture efficiency was down to 40% with C/N = 0.64. Such a trend is understandable since concentrations of both NH_{3, aq} and OH[−] drop dramatically along with the C/N ratio (Figure 2a,b), both of which are two distinctive reactants for CO₂ capture: OH[−] + CO_{2, aq} = HCO₃[−] with the forward rate constant of 1.21 × 10⁵ M^{−1} s^{−120} and NH_{3, aq} + CO_{2, aq} = NH₂COOH with the forward

rate constant of 4.5 × 10² M^{−1} s^{−1}.²¹ Indeed, the experimentally observed time rate of the total concentration of three carbon-centric species (HCO₃[−], NH₂COO[−], and CO₃^{2−}), as a measure of the total reaction of CO₂ capture, showed a sharp declining trend along with the capture time (Figure S3c). Specifically, the fitted total reaction rate decreases from 0.41 M/h at the zeroth hour of CO₂ capture (C/N = 0) to 0.037 M/h (or 91% reduction) at the 12th hour of CO₂ capture (C/N = 0.64). Evidently, a more sophisticated CO₂-capturing system is required to attain even deeper C/N ratios, although no significant technical challenge is anticipated.

By ¹³C NMR spectroscopy, the detected carbon-centric products (HCO₃[−], NH₂COO[−], and CO₃^{2−}) were quantified and plotted against the C/N ratio (Figure 2c). During the C/N ratio range of 0–0.64, the detected concentrations of all products are consistent with the computed trends (Figure 1c). Specifically, at a C/N ratio of 0.64, the observed concentrations for HCO₃[−], NH₂COO[−], and CO₃^{2−} are 1.14, 0.24, and 0.075 M, respectively, which are very consistent with the computed concentrations of 1.28, 0.31, and 0.036 M, correspondingly, at a C/N ratio = 0.64. The deviation for the HCO₃[−] concentration is less than 10%, while variations for the other two products are larger. The observed peak concentration of 0.328 M at C/N ratio = 0.45 for NH₂COO[−] in the capture reaction is very close to the computed peak value (0.339 M) at a near C/N ratio (0.51) for the same product. The peak concentration was also observed for CO₃^{2−}: 0.144 M at C/N ratio = 0.35 in the capture reaction, both of which are higher than the computed values (0.065 M at C/N ratio = 0.22). We believe this discrepancy is largely due to experimental error, considering the low level of concentration and the limited sensitivity of ¹³C NMR.

During the CO₂ capture from the simulated flue gas, the total concentration of NH₃ and NH₄⁺ remained at a high level (from 2.5 to 2.3 M) with a small amount of NH₃ lost by flue gas bubbling (Figure S3a). The ionic concentrations of HCO₃[−], NH₂COO[−], and CO₃^{2−} along with capture time, are shown in Figure S3b.

Currently, many research efforts have been focused on noble metal-based electrocatalysts, such as gold and silver, for CO₂RR to CO, with applications extending to bicarbonate electrolysis systems.^{5,9,22–24} However, these catalysts are not economically viable for large-scale deployment. Furthermore, their catalytic activity can deteriorate rapidly in NH₄⁺-rich environments, such as the NH₄HCO₃ catholyte. This limitation poses a significant challenge for using ammonia as the carbon-capture medium. For example, two Ag-based cathode catalysts (a commercial Ag nanoparticle, or Ag-NP, and a lab-made oxide-derived Ag, or OD-Ag²⁵) were utilized for the electrochemical HCO₃[−]-to-CO conversion to compare NH₄HCO₃ with KHCO₃ as the catholyte at the same concentration of 2.5 M.

Prior to comparing catalytic performance, the operation temperature was optimized using Ni-SAC— a single-atom catalyst introduced in detail below — as the temperature condition established here was consistently applied across all subsequent experiments, including those with Ag-based catalysts. As shown in Figure S4, FE_{CO} of Ni-SAC electrode increased from 42.3% to 56.8% as cell temperature increased from 25 to 40 °C, owing to enriched *i*-CO₂ supply driven by NH₄HCO₃ at elevated temperatures (HCO₃[−] → OH[−] + CO₂, which begins around 36 °C). However, at higher cell

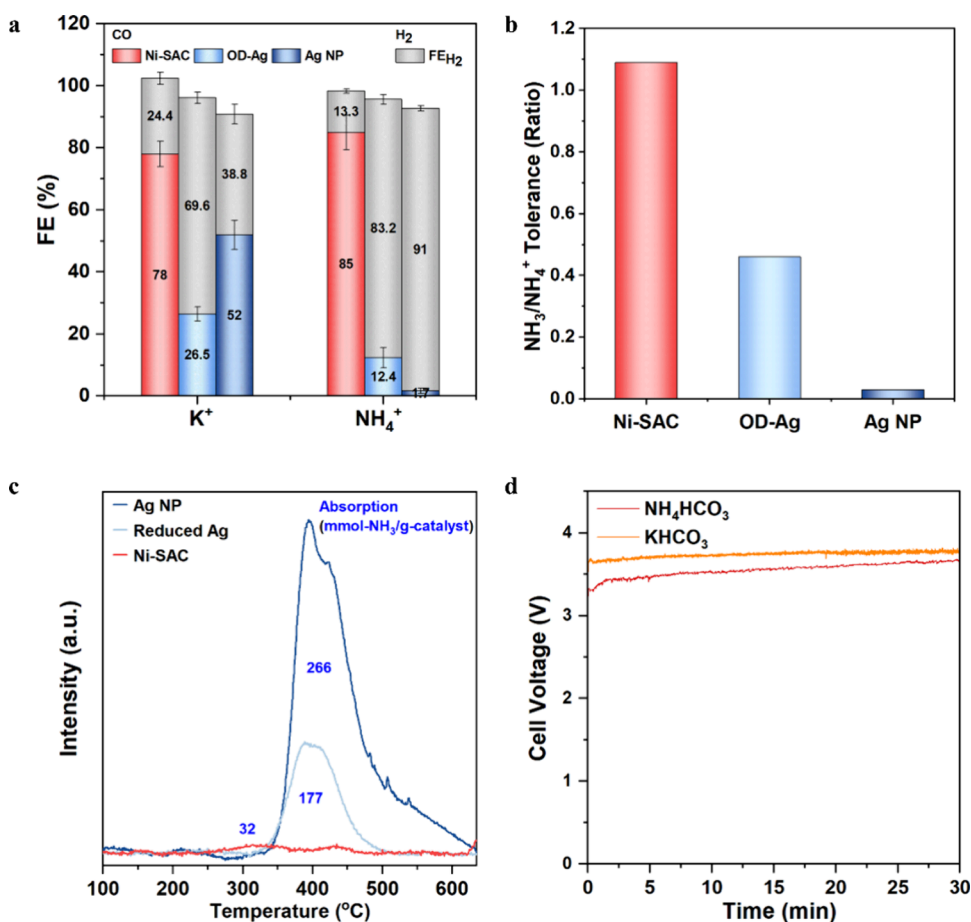


Figure 3. Comparison of the catalytic performance between silver catalysts and Ni-SAC. (a) FE comparison in 2.5 M KHCO₃ and NH₄HCO₃ catholytes under -100 mA/cm^2 at 40 °C. (b) NH₄⁺ tolerance comparison defined by the ratio of FE_{CO} under NH₄⁺ to K⁺. (c) NH₃-TPD analysis of Ag-NP and Ni-SAC. Ammonia adsorption is normalized to the total mass of the catalyst. (d) Cell voltage profiles of Ni-SAC under different cation conditions.

temperature such as 60 °C, FE_{CO} decreased to 45.5% due largely to enhanced HER and decreased CO₂ solubility, consistent with prior reports.²⁶ Therefore, 40 °C was selected as the optimal operation temperature and applied consistently throughout all subsequent experiments.

Both Ag-based catalysts showed moderate Faradaic efficiency toward CO (or FE_{CO} for simplicity, hereinafter) in 2.5 M KHCO₃ at a constant current density of 100 mA/cm²: 52% and 26% on Ag-NP and OD-Ag, respectively (Figure 3a). However, FE_{CO} collapsed to 2% and 12% on Ag-NP and OD-Ag, correspondingly, in 2.5 M NH₄HCO₃ at the same current density, despite the anticipated performance enhancement from NH₄HCO₃ through enhanced *i*-CO₂ generation and lessened electrolyte alkalinity. The bipolar membrane (BPM)-electrolyzer system showed better performance compared to an anion exchange ionomer (AEM)-electrolyzer system with a silver catalyst by mitigating the pH rise by proton delivery from the BPM, retarding the shift of carbonate speciation toward catalytically inactive CO₃²⁻, thereby maintaining a higher fraction of active bicarbonate species in solution.²⁴ In addition, it has been reported that the effective (hydration) radius of cations can affect the electric field near the silver electrodes and the catalytic performances by modulating the charge density at the outer Helmholtz plane (OHP).⁹ The hydrated radii are inversely proportional to the ionic radii for alkali cations. The Ag catalyst showed worse performance under

NH₄⁺ conditions, even though the radius of the NH₄⁺ ion is similar to that of K⁺.^{27,28} Therefore, the poisoning effect on Ag surfaces overruled the potential enhancement by *i*-CO₂ and pH.

In recent years, single metal site catalysts, coordinated with nitrogen ligands and embedded in carbon planes, have emerged as a promising alternative.^{29–32} Among these, the Ni single-atom catalyst (Ni-SAC) has gained enormous attention due to its remarkable CO₂RR activity and CO selectivity compared to conventional metal catalysts.^{7,29,31} This novel electrocatalyst overcomes the limitations of noble metal catalysts. Remarkably, Ni-SAC has demonstrated greater resistance to poisoning in organic amine-rich environments³³ unlike bulk nickel catalysts, suggesting its potential suitability for ammonia-mediated carbon capture and reduction. In particular, a Ni-SAC, structured with one Ni atom coordinated by nitrogen atoms from graphitic moieties supported by ordered mesoporous carbon, was demonstrated to deliver 85% FE_{CO} and 91 mA/cm² of current density under -1.4 V vs RHE in an H-cell filled with a CO₂-saturated 0.5 M KHCO₃ electrolyte (and 95% FE_{CO} and 190 mA/cm² in a gas-diffusion cell).³⁴ Here, we adopt this new family of high-performance catalysts for NH₄HCO₃-to-CO conversion hosted in the NH₄HCO₃ electrolyte in a MEA cell. The detailed characterization methods conducted here confirmed the successful

synthesis with the desirable structures, as evidenced by TEM, BET, XPS, and XRD in Figures S5–S8, respectively.

In sharp contrast to the two Ag catalysts, Ni-SAC delivered 85% FE_{CO} in 2.5 M NH_4HCO_3 , which is even higher than that in 2.5 M $KHCO_3$ (78%) at the same current density of 100 mA/cm². Clearly, Ni-SAC not only is free from ammonia/ammonium poisoning but also benefits from the boosting effects of NH_4HCO_3 .

If we define the “ NH_3/NH_4^+ tolerance” on a catalyst as the ratio of FE_{CO} in NH_4HCO_3 to that in $KHCO_3$, then Ni-SAC has an NH_3/NH_4^+ tolerance of 1.09 or with 9% efficiency enhancement. Following the definition, the NH_3/NH_4^+ tolerance of OD-Ag and Ag-NP is 0.46 and 0.03, respectively (Figure 3b). At the same current density (100 mA/cm²) with the same catalyst (Ni-SAC), the observed cell voltage from the NH_4HCO_3 electrolyte was meaningfully lower than that of $KHCO_3$: 3.35–3.65 V vs 3.65–3.73 V or by 80–300 mV, accordingly (Figure 3d).

To verify whether the captured NH_4HCO_3 is a suitable CO_2 source for its reduction to CO, we conducted electrolysis using two “captured NH_4HCO_3 solutions” obtained from two different capture protocols and compared the results to those of commercial NH_4HCO_3 . First, the “captured NH_4HCO_3 (1.6 M)” solution was obtained by directly absorbing CO_2 from the flue gas by 2.5 M NH_3 solution for 12 h (with the final C/N = 0.64 or 1.6 M NH_4HCO_3). At the same current density of 100 mA/cm², the electrolysis with the “captured NH_4HCO_3 (1.6 M)” solution delivered a reasonably lower FE_{CO} (53%) and a marginally higher cell voltage (3.72 V), (Figure S9), which is 63% of the efficacy of the “commercial NH_4HCO_3 (2.5 M)” (85% of FE_{CO} and 3.68 V of cell voltage). Second, the “captured NH_4HCO_3 (2.5 M)” solution with increased NH_4HCO_3 concentration was prepared by the precipitation-dissolution of solid NH_4HCO_3 obtained via extended CO_2 absorption in 5 M NH_3 solution for 48 h (Figure S10). Having the same concentration of 2.5 M NH_4HCO_3 , the electrolysis with the “captured NH_4HCO_3 (2.5 M)” delivered a marginally lower FE_{CO} (70%) and a higher cell voltage (3.79 V) at the same current density of 100 mA/cm², which is 82% of the efficacy of the “commercial bicarbonate (2.5 M)”. These results demonstrate the technical feasibility of integrating the CO_2 capture with NH_4HCO_3 electrolysis. In addition, direct CO_2 electrolysis using simulated flue gas (containing 20% v/v O_2) was evaluated for comparison (Figure S11). Under these conditions, neither CO_2RR products nor H_2 were detected, indicating that the oxygen-reduction reaction (ORR) predominates. This observation underscores the importance of the proposed integrated CO_2 capture and conversion strategy. By decoupling the capture of CO_2 from gas-phase electrolysis, the BPM-enabled NH_3 -mediated RCC system facilitates CO_2 electroreduction under O_2 -free conditions that are critical for activating Ni-SAC toward the CO_2RR , thereby overcoming a fundamental limitation associated with direct flue-gas-fed electrochemical systems.

Long-term stability tests of the Ni-SAC electrode were conducted at a current density of -50 mA/cm² in a flow cell system (Figure S12). The FE_{CO} stability was defined as the ratio of the FE_{CO} after 30 min to the FE_{CO} measured at each subsequent hour. Over a continuous 6 h operation, the system exhibited stable performance with FE_{CO} stability ranging from 0.9 to 0.8 and an average cell voltage of approximately 3.2 V, indicating sustained catalytic activity and stability. Using NMR spectroscopy, we measured ammonia loss from the NH_4HCO_3

electrolyte during CO -producing electrolysis, and our results showed that, after 6 h at 40 °C, nitrogen loss via NH_3 escape was negligible at only 0.001% (Figure S13).

The sharp distinction in NH_3/NH_4^+ tolerance between Ni-SAC and the Ag catalysts was further supported by ammonia-temperature-programmed desorption (NH_3 -TPD) (Figure 3c). The commercial Ag-NP showed the most NH_3 adsorption of 266 mmol- NH_3 /g-catalyst, followed by the reduced Ag (mimicking the OD-Ag) of 177 mmol- NH_3 /g-catalyst, both of which culminated adsorption peaks around 400 °C. By stark contrast, a significantly lower amount of adsorption was observed on Ni-SAC: 32 mmol- NH_3 /g-catalyst or 12–18% that of Ag catalysts. In addition, no clear adsorption peak was detected on Ni-SAC. Those NH_3 -TPD results confirmed the much weaker metal–N binding on Ni-SAC than on Ag. This adsorption adversely affected the catalytic activity of silver and the CO_2RR performance.

To acquire deeper insights into the effects of NH_4^+ cations on Ni-SAC and Ag catalysts, we performed DFT calculations. The DFT-calculated adsorption energies of nonhydrated NH_4^+ , hydrated NH_4^+ ($NH_4^+ \cdot 3H_2O$), CO_2 , and H_2O on both Ni-SAC and Ag(111) surfaces are presented in Table 1

Table 1. Adsorption Enthalpies (in eV) of NH_4^+ , $NH_4^+ \cdot 3H_2O$, H_2O , and CO_2 on Ni-SAC and Ag(111) Surfaces

Surface	NH_4^+	$NH_4^+ \cdot 3H_2O$	H_2O	CO_2
Ni-SAC	−1.22	−2.31	−0.19	−0.17
Ag(111)	−2.12	−3.31	−0.32	−0.23

with the corresponding optimized structures shown in Figure S14. Here, we considered the microsolvation of three H_2O molecules with three N–H groups, since NH_4^+ is expected to form hydrogen bonds between its N–H groups and H_2O molecules. The computation results clearly show that the adsorption of nonhydrated NH_4^+ is significantly loosened on Ni-SAC compared to Ag(111) with -1.22 and -2.12 eV of adsorption enthalpy, respectively, or 0.90 eV relaxed. Very similarly, the adsorption of hydrated NH_4^+ ($NH_4^+ \cdot 3H_2O$) is loosened by 1.00 eV: -2.31 eV on Ni-SAC vs -3.31 eV on Ag(111). Such a loosened adsorption of NH_4^+ (both hydrated and nonhydrated) on Ni-SAC against Ag(111) in the DFT study is fundamentally consistent with the distinctive thermal adsorption of ammonia in the NH_3 -TPD observation.

The binding enthalpy of CO_2 and H_2O was also computed on both Ni-SAC and Ag(111) (Table 1). The adsorption of CO_2 molecules on both surfaces is similarly weak with adsorption enthalpies of -0.17 and -0.23 eV on Ni-SAC and Ag(111), respectively, largely because of the nonpolar nature of CO_2 . The adsorption of H_2O molecules is slightly stronger than that of CO_2 on both surfaces: 0.02 and 0.10 eV of more negative enthalpy on Ni-SAC and Ag(111), correspondingly. Despite significantly weakened binding compared with Ag(111), Ni-SAC still possesses much stronger adsorption toward NH_4^+ than CO_2 (and H_2O as well) by 1.05 eV (and 1.03 eV accordingly). Therefore, NH_4^+ is expected to compete with the CO_2 molecules on Ni-SAC with some level of surface blocking, suggesting that a catalyst with even less NH_4^+ adsorption may drastically enhance FE_{CO} .

Due to the simultaneous adsorption of both H_2O and NH_4^+ on the two surfaces, the dynamic competition between them at the water–solid interface is complex and likely significant. To capture this dynamic behavior, ab initio molecular dynamics

(AIMD) simulations were conducted for each system, incorporating three explicit H₂O layers on the catalyst surface. The vertical distance between the N atom in NH₄⁺ and the surface metal atom was calculated and is shown in Figure 4 for Ni-SAC and Ag(111).

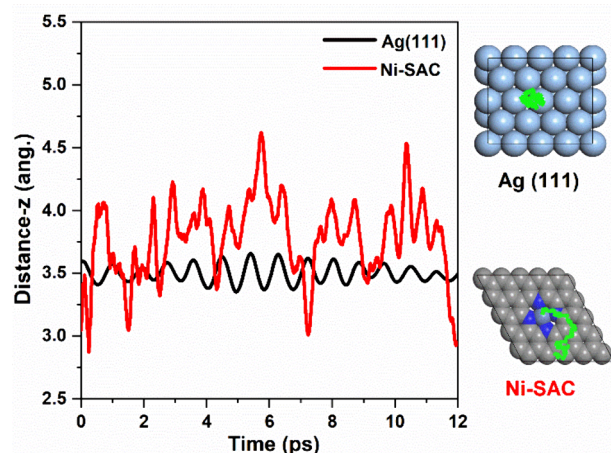


Figure 4. Vertical (z) distance of the N atom in NH₄⁺ with respect to the catalyst surface in the AIMD simulations. The x and y positions of the N in NH₄⁺ during the AIMD simulation over Ag(111) and Ni-SAC are shown on the right. Nitrogen and Ni are also highlighted within the graphitic carbon framework.

On Ni-SAC, the NH₄⁺ ion quickly drifts away from the Ni center and diffuses over the graphitic surface in the early stages of the AIMD simulations. This behavior makes the Ni center available for CO₂ adsorption to compete with NH₄⁺. Due to the weak interaction between water and the graphitic carbon surface, the NH₄⁺ ion is trapped at the interface (at least within the simulation time), reducing the contact between water and carbon. The NH₄⁺ ion fluctuates within a wide range of 2.8–4.7 Å, at an average of 3.77 Å, above the Ni-SAC surface. As opposed to the dramatic variation in N-metal distance on Ni-SAC, NH₄⁺ remains adsorbed on the Ag(111) surface throughout the entire simulation period (about 20 ps), maintaining a position around 3.48 ± 0.15 Å above the Ag surface with the smallest fluctuation in the z direction. The AIMD simulation results consolidate the much weaker interaction of NH₄⁺ on Ni-SAC than that on Ag(111). With such a small and steady distance, the Ag surface remains enriched by NH₄⁺, which hinders the diffusion of CO₂ to reach the metal surface and react, thus deciphering the suppressed CO₂ reduction on Ag-NP observed in the presence of NH₄⁺. These studies provide a molecular-scale understanding of NH₄HCO₃ electrolysis, revealing unique molecule–catalyst interactions.

To better understand the economic viability of the proposed tandem process of CO₂ → NH₄HCO₃ → CO, a model of techno-economic analysis (TEA) was established in this study by extending our recent work in TEA for electrodialysis and electrolysis.³⁵ Consistently, \$/kmol-CO was adopted as the functional unit throughout the TEA framework, and the dollar value is based on the current buying power in 2025. As a measure of the overall manufacturing cost, the “levelized total cost” (LTC) was obtained by summing the “operational expense” (OPEX) and the “levelized capital cost” (LCC) in the same functional unit.

For OPEX, five separate modules were considered: electrolysis of NH₄HCO₃ for CO production (OPEX-el), cooling for CO₂-capturing solution (OPEX-c), heating for electrolysis at desirable cell temperature (OPEX-h), pumping for electrolyte management (OPEX-p), and others for unidentified yet necessary expenses (OPEX-o). Simply, OPEX = OPEX-el + OPEX-c + OPEX-h + OPEX-p + OPEX-o. OPEX-el was quantified as \$15.97/kmol-CO based on the typical cell voltage of 3.64 V (uncompensated) from the electrolysis cell and the typical FE_{CO} of 85.5%. OPEX-c was estimated as \$0.46/kmol-CO based on 20 °C of temperature drop (from 25 to 5 °C) with 2 M NH₃ and 50% HCO₃[−] utilization. OPEX-h was calculated as \$1.22/kmol-CO based on 15 °C of temperature increase (from 25 to 40 °C) with 2 M NH₃ and 50% HCO₃[−] utilization. OPEX-p was determined as \$1.55/kmol-CO based on 4 cm/s of nominal velocity and 50% pressure drop. The last module, OPEX-o, was assumed as 5% of the four modules: \$0.88/kmol-CO. Note that a flat rate of electricity cost (\$0.07/kWh) was adopted here consistently for all OPEX modules. Therefore, the total amount of OPEX was found to be \$18.55/kmol-CO, 86% of which comes from the electrolysis module (Figure 5a).

Prior to LCC estimation, capital cost analysis was performed based on a customized medium-size electrolyzer with 1 m² of effective cell area and 3 kW of power rating (500 cm²/cell × 100 mA/cm² × 3 V × 20 cells/stack). The cost of all identified materials and ancillary/auxiliary parts/components was estimated to be \$8,151 per system to which the commercial bipolar membrane contributes dominantly (64%, \$5,216/m²). Next, considering all unidentified parts (10%) and all other associated costs,³⁰ the total capital cost of such an electrolyzer system was projected to be \$11,746 per system. Based on the total capital cost (\$11,746 per system) and the standard capital recovery method, the LCC for the electrolysis system was calculated to be \$6.88/kmol-CO on the following assumptions: 20 years of service time, 10% as the cost ratio of maintenance to the system, 3% of annual discount rate,³¹ 90.4% of capacity factor, and 85.5% of FE_{CO}. Thanks to the inexpensive materials (such as Ni-SAC as the cathode catalyst, nickel foam as the anode material, and carbon substrates) used to construct the electrolysis system, LCC remains at a low level. Finally, the LTC = OPEX + LCC = \$18.55 + \$6.88 = \$25.43/kmol-CO for the electrolysis system with Ni-SAC as the cathode catalyst. Clearly, LCC occupies a small portion of LTC (27%) (Figure 5b).

We also examined the impact of both cell voltage (from 2 to 5 V) and FE_{CO} (from 20% to 100%) on the LTC, as shown in the contour map (Figure 5c). Clearly, lowering cell voltage and raising FE_{CO} reduce the manufacturing cost of CO. Specifically, under the same electrolysis voltage of 3.5 V, the LTC will climb from \$23.63/kmol-CO with 90% FE_{CO} to \$41.12/kmol-CO with 50% FE_{CO}. With the same FE_{CO} of 90%, LTC will fall from \$28.01/kmol-CO under 4.5 V to \$19.25/kmol-CO under 2.5 V. LTC is largely controlled by the OPEX, suggesting that future improvement should be primarily focused on lowering the cell voltage. Meanwhile, utilizing low cost and renewable electricity may significantly reduce LTC, considering heavy energy consumption. The TEA framework established here clearly reveals that increasing the operational current density or lowering materials' cost is deemed ineffective to cut down on LTC, because of the small contribution from LCC (21%). With the typical cell performance (3.80 V of electrolysis voltage and 12% of FE_{CO}), the LTC on OD-Ag obtained from

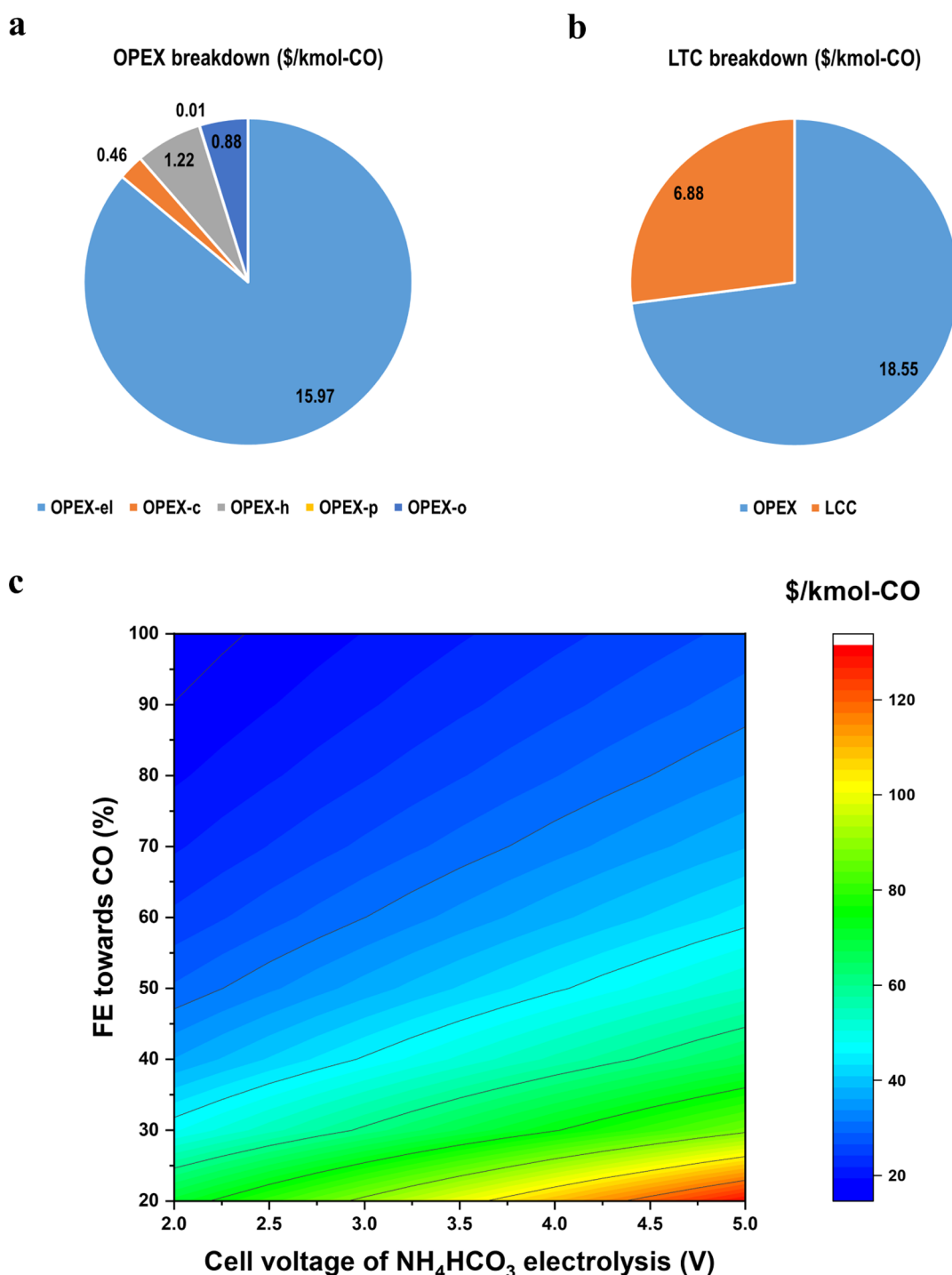


Figure 5. Techno-economic analysis of captured CO_2 reduction with NH_4HCO_3 electrolysis. (a) Operational Expense (OPEX), a measure of the total operating cost. (b) Levelized Total Cost (LTC), a measure of the total manufacturing cost of CO in \$/kmol-CO. Levelized Capital Cost (LCC) is a measure of the normalized cost from capital investment (stack cost, installation, maintenance, and finance). (c) Contour plot of LCC against FE_{CO} and cell voltage of NH_4HCO_3 electrolysis (\$0.07/kWh of electricity cost).

our TEA model was \$163.55/kmol-CO or 6.4 times that on Ni-SAC (\$25.43/kmol-CO). OPEX dramatically increased to \$126.59/kmol-CO on OD-Ag from \$18.55/kmol-CO on Ni-SAC, while LCC also inflated to \$36.95/kmol-CO on OD-Ag from \$6.88/kmol-CO.

Our results establish the feasibility of an NH_3 -mediated tandem RCC system that couples CO_2 capture and electrochemical conversion in a single framework. By correlating speciation simulations with experimental observations, we

demonstrate how capture depth governs the distribution of reactive carbon–nitrogen species and directly influences electrolysis outcomes. The dramatic contrast between Ag-based catalysts and Ni-SAC highlights a critical design principle for RCC: while Ag suffers from severe ammonium poisoning that blocks CO_2 reduction, Ni-SAC not only resists deactivation but also benefits from enhanced CO selectivity and lower cell voltages in the NH_4HCO_3 electrolyte. These findings, supported by spectroscopy and simulations, reveal

that single-atom Ni centers provide a catalytic platform that is robust and compatible with ammonia-based capture environments. From a techno-economic perspective, the analysis indicates that improvements in energy efficiency and selectivity—rather than higher current densities or lower material costs—are the most decisive levers for reducing the cost of CO production. The demonstrated tolerance and promotion effects of Ni-SAC thus address both the scientific and practical barriers that have hindered RCC deployment. Looking forward, extending this concept to higher-value products and validating long-term performance under realistic flue gas conditions could position ammonia-mediated RCC as a scalable strategy for carbon utilization.

■ ASSOCIATED CONTENT

SI Supporting Information

The Supporting Information is available free of charge at <https://pubs.acs.org/doi/10.1021/acsenergylett.5c04265>.

Speciation computation, experimental methods, techno-economic analysis (TEA), and supporting figures, including a photo of the CO₂ capture system, ¹³C NMR spectra, TEM images, BET analysis, XPS spectra, XRD analysis, and additional experimental data (PDF)

■ AUTHOR INFORMATION

Corresponding Authors

Wenzhen Li – Department of Chemical and Biological Engineering, Iowa State University, Ames, Iowa 50011, United States; orcid.org/0000-0002-1020-5187; Email: wzli@iastate.edu

Shuang Gu – Department of Mechanical Engineering, Wichita State University, Wichita, Kansas 67260, United States; orcid.org/0000-0003-1532-0093; Email: Shuang.Gu@wichita.edu

Bin Wang – School of Sustainable Chemical, Biological and Materials Engineering, University of Oklahoma, Norman, Oklahoma 73019, United States; Present Address: Department of Chemical and Biological Engineering, Tufts University, 200 Boston Avenue, Medford, MA 02155, United States; orcid.org/0000-0001-8246-1422; Email: Bin.Wang@tufts.edu

Authors

Sujin Kang – Department of Chemical and Biological Engineering, Iowa State University, Ames, Iowa 50011, United States

Shoutian Sun – School of Sustainable Chemical, Biological and Materials Engineering, University of Oklahoma, Norman, Oklahoma 73019, United States

Lun An – DOE Ames National Laboratory, Ames, Iowa 50011, United States; orcid.org/0000-0003-2146-1490

Jie Zhang – DOE Ames National Laboratory, Ames, Iowa 50011, United States

Long Qi – DOE Ames National Laboratory, Ames, Iowa 50011, United States; orcid.org/0000-0002-1213-2946

Wenyu Huang – Department of Chemistry, Iowa State University, Ames, Iowa 50011, United States; orcid.org/0000-0003-2327-7259

Complete contact information is available at: <https://pubs.acs.org/doi/10.1021/acsenergylett.5c04265>

Author Contributions

#S.K. and S.S. are co-first authors. S.K., S.G., and W.L. initiated the project and conceptualized the research idea. S.K. designed and performed the experiments. S.G. performed the computation of the system species. S.S. performed DFT calculations and AIMD simulations. L.A. synthesized and characterized catalysts. J.Z. performed TPD analysis. S.G. performed the techno-economic analysis. S.K., S.S., L.A., and S.G. prepared the manuscript. L.Q., W.H., B.W., S.G., and W.L. proposed and supervised the project. All authors collaborated in discussions and contributed to the manuscript's writing and review.

Notes

The authors declare no competing financial interest.

■ ACKNOWLEDGMENTS

This research was supported by the U.S. National Science Foundation (NSF) agency through ECO-CBET (2219162 & 2219172), EPSCoR RII-Track-2 FEC (2316481 & 2316482), and Future Manufacturing (FMRG 2428214) programs and by the U.S. DOE agency through Office of Science from both EPSCoR program (DE-SC0025376) and the Division of Chemical Sciences, Geosciences, and Biosciences (DE-SC0018284). All first-principles calculations were performed at the OU Supercomputing Center for Education & Research and the National Energy Research Scientific Computing Center (NERSC), a U.S. DOE Office of Science User Facility. L.A., L.Q., and W.H. acknowledge the Laboratory-Directed Research and Development program at Ames National Laboratory for the design and synthesis of carbon materials. The Ames Laboratory is operated for the U.S. DOE by Iowa State University under contract no. DE-AC02-07CH11358. S.G. appreciates the Sam Bloomfield Chair Professor endowment. W.L. is grateful to his Manley Hoppe Professor endowment and ISU-VPR Biobased Products funding from Iowa State University. We are grateful to Dr. Dapeng Kiang for XPS characterizations, and we also thank the fruitful discussion with Dr. Yifu Chen, Dr. Hengzhou Liu, Dr. Qiqi Mao, Prof. Gang Wu, Tianlei Li, Xiaopeng Liu, Mohammad Albloushi, Rod Alexei De Guzman, and Huu Huy Nguyen.

■ REFERENCES

- (1) Nielsen, D. U.; Hu, X.-M.; Daasbjerg, K.; Skrydstrup, T. Chemically and electrochemically catalysed conversion of CO₂ to CO with follow-up utilization to value-added chemicals. *Nat. Catal.* **2018**, *1* (4), 244–254.
- (2) Deutsch, T. G.; Baker, S.; Agbo, P.; Kauffman, D. R.; Vickers, J.; Schaidle, J. A. *Summary Report of the Reactive CO₂ Capture: Process Integration for the New Carbon Economy Workshop*; National Renewable Energy Laboratory (NREL): Golden, CO (United States), 2020.
- (3) Zhang, K.; Guo, D.; Wang, X.; Qin, Y.; Hu, L.; Zhang, Y.; Zou, R.; Gao, S. Sustainable CO₂ management through integrated CO₂ capture and conversion. *J. CO₂ Util.* **2023**, *72*, No. 102493.
- (4) Gao, W.; Liang, S.; Wang, R.; Jiang, Q.; Zhang, Y.; Zheng, Q.; Xie, B.; Toe, C. Y.; Zhu, X.; Wang, J. Industrial carbon dioxide capture and utilization: state of the art and future challenges. *Chem. Soc. Rev.* **2020**, *49* (23), 8584–8686.
- (5) Lees, E. W.; Goldman, M.; Fink, A. G.; Dvorak, D. J.; Salvatore, D. A.; Zhang, Z.; Loo, N. W.; Berlinguette, C. P. Electrodes designed for converting bicarbonate into CO. *ACS Energy Letters* **2020**, *5* (7), 2165–2173.
- (6) Lee, J.; Liu, H.; Li, W. Bicarbonate Electroreduction to Multicarbon Products Enabled by Cu/Ag Bilayer Electrodes and

- Tailored Microenvironments. *ChemSusChem* **2022**, *15* (22), No. e202201329.
- (7) Song, H.; Fernández, C. A.; Choi, H.; Huang, P.-W.; Oh, J.; Hatzell, M. C. Integrated carbon capture and CO production from bicarbonates through bipolar membrane electrolysis. *Energy Environ. Sci.* **2024**, *17* (10), 3570–3579.
- (8) Zhang, Z.; Melo, L.; Janssonius, R. P.; Habibzadeh, F.; Grant, E. R.; Berlinguette, C. P. pH Matters When Reducing CO₂ in an Electrochemical Flow Cell. *ACS Energy Lett.* **2020**, *5* (10), 3101–3107.
- (9) Fink, A. G.; Lees, E. W.; Zhang, Z.; Ren, S.; Delima, R. S.; Berlinguette, C. P. Impact of alkali cation identity on the conversion of HCO₃[−] to CO in bicarbonate electrolyzers. *ChemElectroChem.* **2021**, *8* (11), 2094–2100.
- (10) Zhang, Z.; Melo, L.; Janssonius, R. P.; Habibzadeh, F.; Grant, E. R.; Berlinguette, C. P. pH matters when reducing CO₂ in an electrochemical flow cell. *ACS Energy Letters* **2020**, *5* (10), 3101–3107.
- (11) Yoshizawa, A.; Higashi, M.; Anzai, A.; Yamauchi, M. A membrane electrode assembly-type cell designed for selective CO production from bicarbonate electrolyte and air containing CO₂ mixed gas. *Energy Adv.* **2024**, *3* (4), 778–783.
- (12) Shen, M.; Ji, L.; Cheng, D.; Wang, Z.; Xue, Q.; Feng, S.; Luo, Y.; Chen, S.; Wang, J.; Zheng, H. Hierarchical design enables sufficient activated CO₂ for efficient electrolysis of bicarbonate to CO. *Joule* **2024**, *8* (7), 1999–2015.
- (13) *Green Ammonia: zero-carbon fertiliser, fuel and energy store*; The Royal Society, 2020.
- (14) Liu, H.; Chen, Y.; Lee, J.; Gu, S.; Li, W. Ammonia-Mediated CO₂ Capture and Direct Electroreduction to Formate. *ACS Energy Lett.* **2022**, *7* (12), 4483–4489.
- (15) Li, T.; Subedi, N.; Kang, S.; Mao, Q.; Fei, Y.; Gu, S.; Li, W. High-current-density electrosynthesis of formate from captured CO₂ solution by MOF-derived bismuth nanosheets. *Chem. Eng. J.* **2025**, *519*, No. 165272.
- (16) Bai, H.; Yeh, A. C. Removal of CO₂ greenhouse gas by ammonia scrubbing. *Ind. Eng. Chem. Res.* **1997**, *36* (6), 2490–2493.
- (17) Mani, F.; Peruzzini, M.; Stoppioni, P. CO₂ absorption by aqueous NH₃ solutions: speciation of ammonium carbamate, bicarbonate and carbonate by a ¹³C NMR study. *Green Chem.* **2006**, *8* (11), 995–1000.
- (18) Ma, S.; Fan, S.; Chen, L.; Yang, P.; Chen, G.; Ma, J. Absorption Kinetics of CO₂ in Aqueous Ammonia with High Load and Salinity. *Ind. Eng. Chem. Res.* **2023**, *62* (19), 7384–7396.
- (19) Prajapati, A.; Sartape, R.; Galante, M. T.; Xie, J.; Leung, S. L.; Bessa, I.; Andrade, M. H. S.; Somich, R. T.; Rebouças, M. V.; Hutras, G. T.; Diniz, N.; Singh, M. R. Fully-integrated electrochemical system that captures CO₂ from flue gas to produce value-added chemicals at ambient conditions. *Energy Environ. Sci.* **2022**, *15* (12), 5105–5117.
- (20) McCann, N.; Phan, D.; Wang, X.; Conway, W.; Burns, R.; Attalla, M.; Puxty, G.; Maeder, M. Kinetics and mechanism of carbamate formation from CO_{2(aq)}, carbonate species, and monoethanolamine in aqueous solution. *J. Phys. Chem. A* **2009**, *113* (17), 5022–5029.
- (21) Wang, X.; Conway, W.; Fernandes, D.; Lawrance, G.; Burns, R.; Puxty, G.; Maeder, M. Kinetics of the reversible reaction of CO_{2(aq)} with ammonia in aqueous solution. *J. Phys. Chem. A* **2011**, *115* (24), 6405–6412.
- (22) Wang, W.; Gong, S.; Wang, H.; Tan, Y.; Zhu, X.; Wang, X.; Liu, J.; Yu, W.; Zhu, G.; Lv, X. Surface-modified silver aerogels combining interfacial regulation for electrocatalytic CO₂ reduction under large current density. *Chem. Eng. J.* **2024**, *490*, No. 151849.
- (23) Zhang, Z.; Lees, E. W.; Habibzadeh, F.; Salvatore, D. A.; Ren, S.; Simpson, G. L.; Wheeler, D. G.; Liu, A.; Berlinguette, C. P. Porous metal electrodes enable efficient electrolysis of carbon capture solutions. *Energy Environ. Sci.* **2022**, *15* (2), 705–713.
- (24) Li, T.; Lees, E. W.; Goldman, M.; Salvatore, D. A.; Weekes, D. M.; Berlinguette, C. P. Electrolytic Conversion of Bicarbonate into CO in a Flow Cell. *Joule* **2019**, *3* (6), 1487–1497.
- (25) Liu, H.; Park, J.; Chen, Y.; Qiu, Y.; Cheng, Y.; Srivastava, K.; Gu, S.; Shanks, B. H.; Roling, L. T.; Li, W. Electrocatalytic Nitrate Reduction on Oxide-Derived Silver with Tunable Selectivity to Nitrite and Ammonia. *ACS Catal.* **2021**, *11* (14), 8431–8442.
- (26) (a) Kim, J. H.; Jang, H.; Bak, G.; Choi, W.; Yun, H.; Lee, E.; Kim, D.; Kim, J.; Lee, S. Y.; Hwang, Y. J. The insensitive cation effect on a single atom Ni catalyst allows selective electrochemical conversion of captured CO₂ in universal media. *Energy Environ. Sci.* **2022**, *15* (10), 4301–4312. (b) Kang, S.; An, L.; Li, T.; Qi, L.; Huang, W.; Li, W. Electrochemical Reduction of Ammonia Captured CO₂ to CO over Nickel Single-Atom Catalyst. *Green Chem.* **2025**, *27*, 13375–13384.
- (27) Wall, S. Ammonium transport and the role of the Na, K-ATPase. *Miner. Electrolyte Metab.* **1996**, *22* (5–6), 311–317.
- (28) Han, J.; Varzi, A.; Passerini, S. The emergence of aqueous ammonium-ion batteries. *Angew. Chem.* **2022**, *134* (14), No. e202115046.
- (29) Li, Y.; Adli, N. M.; Shan, W.; Wang, M.; Zachman, M. J.; Hwang, S.; Tabassum, H.; Karakalos, S.; Feng, Z.; Wang, G.; Li, Y. C.; Wu, G. Atomically dispersed single Ni site catalysts for high-efficiency CO₂ electroreduction at industrial-level current densities. *Energy Environ. Sci.* **2022**, *15* (5), 2108–2119.
- (30) Yin, Z.; Yu, J.; Xie, Z.; Yu, S. W.; Zhang, L.; Akauola, T.; Chen, J. G.; Huang, W.; Qi, L.; Zhang, S. Hybrid Catalyst Coupling Single-Atom Ni and Nanoscale Cu for Efficient CO₂ Electroreduction to Ethylene. *J. Am. Chem. Soc.* **2022**, *144* (45), 20931–20938.
- (31) Yue, P.; Xiong, K.; Ma, L.; Li, J.; Zhang, L.; Zhu, X.; Fu, Q.; Liao, Q. MOF-derived Ni single-atom catalyst with abundant mesopores for efficient mass transport in electrolytic bicarbonate conversion. *ACS Appl. Mater. Interfaces* **2022**, *14* (49), 54840–54847.
- (32) Chen, Z.; Zhang, X.; Liu, W.; Jiao, M.; Mou, K.; Zhang, X.; Liu, L. Amination strategy to boost the CO₂ electroreduction current density of M–N/C single-atom catalysts to the industrial application level. *Energy Environ. Sci.* **2021**, *14* (4), 2349–2356.
- (33) Kim, J. H.; Jang, H.; Bak, G.; Choi, W.; Yun, H.; Lee, E.; Kim, D.; Kim, J.; Lee, S. Y.; Hwang, Y. J. The insensitive cation effect on a single atom Ni catalyst allows selective electrochemical conversion of captured CO₂ in universal media. *Energy Environ. Sci.* **2022**, *15* (10), 4301–4312.
- (34) Luo, Z.; Yin, Z.; Yu, J.; Yan, Y.; Hu, B.; Nie, R.; Kolln, A. F.; Wu, X.; Behera, R. K.; Chen, M.; Zhou, L.; Liu, F.; Wang, B.; Huang, W.; Zhang, S.; Qi, L. General Synthetic Strategy to Ordered Mesoporous Carbon Catalysts with Single-Atom Metal Sites for Electrochemical CO₂ Reduction. *Small* **2022**, *18* (16), 2107799.
- (35) Chen, Y.; Ammari-Azar, P.; Liu, H.; Lee, J.; Xi, Y.; Castellano, M. J.; Gu, S.; Li, W. Sustainable waste-nitrogen upcycling enabled by low-concentration nitrate electro dialysis and high-performance ammonia electrosynthesis. *EES Catalysis* **2023**, *1* (4), 504–515.